EFDA–JET–PR(11)47

T. Gassner, J. Eriksson, C. Hellesen, V.G. Kiptily, S.D. Pinches, K. Schoepf, S.E. Sharapov and JET EFDA contributors

Deuterium Beam Acceleration with 3rd Harmonic ICRH in Joint European Torus: Sawtooth Stabilization and Alfvén Eigenmodes

Deuterium Beam Acceleration with 3rd Harmonic ICRH in Joint European Torus: Sawtooth Stabilization and Alfvén Eigenmodes

T. Gassner, J. Eriksson[2], C. Hellesen[3], V.G. Kiptily[3], S.D. Pinches[3], K. Schoepf[1], S.E. Sharapov[3] and JET EFDA contributors*

JET-EFDA, Culham Science Centre, OX14 3DB, Abingdon, UK

[1]*EURATOM-OEAW Fusion Association, Institute for Theoretical Physics, University of Innsbruck, A-6020, Austria*
[2]*EURATOM-VR, Department of Physics and Astronomy, Uppsala University, SE-75120, Uppsala, Sweden*
[3]*EURATOM-CCFE Fusion Association, Culham Science Centre, OX14 3DB, Abingdon, OXON, UK*
** See annex of F. Romanelli et al, "Overview of JET Results",*
(23rd IAEA Fusion Energy Conference, Daejon, Republic of Korea (2010)).

Preprint of Paper to be submitted for publication in
Physics of Plasmas

ABSTRACT

Experiments on accelerating NBI-produced deuterium (D) beam ions from their injection energy of ~ 110 keV up to the MeV energy range with 3rd harmonic ICRH were performed on the Joint European Torus. A renewed set of nuclear diagnostics was used for analysing fast D ions during sawtooth stabilization, monster sawtooth crashes, and during excitation of Alfvén eigenmodes (AEs) residing inside the $q = 1$ radius. The measurements and modeling of the fast ions with the nonlinear HAGIS code show that monster sawtooth crashes are strongly facilitated by the AE-induced re-distribution of the fast D ions from inside the $q = 1$ radius to the plasma edge.

1. INTRODUCTION

In a next-step burning plasma experiment fusion-born alpha-particles are expected to affect significantly magnetohydrodynamical (MHD) modes. Sawtooth oscillations, which are periodic relaxation oscillations of central temperature, density, and other plasma parameters, are one of the main instabilities in tokamak plasmas with safety factor $q(0) < 1$. In plasmas with significant auxiliary heating the sawteeth could be effectively suppressed for long periods by energetic particles [6, 24] inside the $q = 1$ radius. These sawteeth have a longer period and saturated or decreasing central electron temperature, $dT_e(0)/dt \leq 0$. They are called "monster" sawteeth. A similar stabilization of sawteeth by fusion alpha-particles is predicted to play a major role in burning plasma ITER experiment[25]. Although the monster sawteeth have much longer periods between sawtooth crashes, the crashes do happen and they produce a more significant drop in electron temperature. Also, the monster sawtooth crashes occur on a time scale about an order of magnitude shorter than the crashes of sawteeth in plasmas with Ohmic heating.

For explaining why the monster sawtooth crash does occur though the stabilising energetic particle population is still sustained by auxiliary heating, it was suggested [10, 3] that Alfvén instabilities inside the $q = 1$ radius observed prior to the crashes may play a role since they share with the sawtooth the same energetic particle population and have the ability to expel resonant fast ions from inside the $q = 1$ radius. This interpretation was further supported by experimental observations [29, 28] on the Joint European Torus (JET) [26] during experiments with hydrogen minority ion cyclotron resonance heating (ICRH) stabilising sawteeth. Significant decrease in gamma-ray emission caused by fast hydrogen ions was detected correlating with the onset of the "tornado" modes [27] (Alfvén eigenmodes residing inside the $q = 1$ radius [21]) followed by the monster sawtooth crash. It was however difficult to perform an unambiguous modeling of the fast hydrogen redistribution due to the AEs in these observations on JET since the nuclear gamma-rays coming from ^{12}C(p,p'γ)^{12}C reaction had a threshold energy ~ 5 MeV for hydrogen ions, and this value was well above the typical energy of fast ions resonating with AEs [29, 28].

Recently, experiments were performed on JET with a deuterium beam accelerated up to the MeV range by 3rd harmonic ICRH. In these experiments, sawtooth stabilization by fast D ions as well as “tornado” mode excitation by D ions were observed followed by monster sawtooth crashes. Although the physics of both sawtooth stabilization and AE excitation in this experiment is expected to be the same as in the experiment with fast hydrogen, the use of fast deuterium significantly expands the opportunities for diagnosing fast ions. First, deuterium ions provide a source of DD neutrons. These are born at energy 2.5 MeV in the centre-of-mass reference frame, but have much broader energy spectrum and much higher cross-section of DD nuclear reaction if fast deuterium is involved [12]. Second, fast deuterium also gives rise to intense gamma-ray emission from the reaction ^{12}C(D,p)^{13}C. The threshold energy for D ions in this reaction is ~ 700 keV, i.e. much lower than ~ 5 MeV for the hydrogen experiments, and very close to the energy of the resonance with Alfvén waves. Therefore one concludes that the technique of fast ion sawtooth stabilization in this case is much more suitable for diagnosing the processes involving fast ions and Alfvén waves.

It is important to note here that resonant interaction between shear Alfvén waves and energetic ions is a key burning plasma issue [14] in its own right (i.e. it is important not only in conjunction with the sawtooth problem). Since the alpha-particles born in fusion DT reactions have super-Alfvénic birth energy of 3.52 MeV, during the slowing-down process they cross the Alfvén resonance

$$V_{\parallel\alpha} = V_A \tag{1}$$

and may release their free energy associated with the radial gradient of alpha-particle pressure by exciting Alfvén waves [1]. Toroidal Alfvén eigenmodes (TAEs) [5] whose frequencies reside within so-called toroidicity-induced “gaps” in the Alfvén continuum have a lower damping rate and hence can be most easily excited by alpha-particles in burning plasmas [8]. It has been long recognized that such excitation of TAEs may re-distribute energetic particles in radius causing clump of the plasma burn and damages to the first wall due to increased fast ion losses [30].

A significant effort was made for developing numerical tools required for modeling of such TAE-induced losses prior to the high-power DT experiments on TFTR [31] and on JET. At JET/Culham, the particle following code HAGIS [23] has been developed allowing computation of the particle orbits in the presence of Alfvén eigenmodes in a real tokamak equilibrium. The equilibrium code HELENA [13] and the spectral MHD codes CASTOR [16] and MISHKA [22] are used for the MHD input to HAGIS, while the fast ion drift distribution function is prescribed via the variables of the ion energy, toroidal angular momentum, and magnetic moment.

Aim of the present work is to investigate, using the HAGIS code, the effect of TAEs driven unstable inside the $q = 1$ radius on the sawtooth stability [10, 3, 29, 28] in the experiments with fast deuterium ions driven by the mixture of NBI and 3$^{\text{rd}}$ harmonic ICRH. Recent JET enhancement of fusion diagnostics has expanded significantly the amount and quality of the data on energetic ions, so that some new time-resolved measurements of the fast ion distribution function became possible. In particular, the new neutron spectrometer TOFOR [15] can now provide data on the energy distribution function of the fast deuterium ions from measurements of the DD fusion-born neutrons. Section II of this paper presents the experimental set-up, a description of the main diagnostics and the data obtained in these JET experiments.

A range of codes is involved in the accurate reconstruction the plasma equilibrium as well as the TAE and tornado modes, a process which is presented in detail in Section III.

The sawtooth stabilization is achieved in these JET experiments by trapped energetic deuterium ions. These trapped ions change the sign of the parallel velocity along their orbits and cannot resonate with Alfvén eigenmodes via Landau interaction (1) as the passing ions do. Instead, the trapped ion resonance condition

$$\Omega \equiv \omega - n\langle\dot{\varphi}\rangle - p\langle\dot{\vartheta}\rangle = 0 \tag{2}$$

has to be satisfied, where ω, n are the frequency and toroidal mode number of the resonating Alfvén eigenmode, $\langle\dot{\varphi}\rangle$ is the orbit-averaged frequency of toroidal motion of the fast ion (toroidal precessional frequency), $\langle\dot{\vartheta}\rangle$ is the orbit averaged frequency of poloidal motion of the ion (bounce frequency), and p is an integer number. Although an elegant analytical theory [7, 9] was developed for the interactions between trapped energetic ions and Alfvén eigenmodes, for real tokamak geometry with non-circular cross-section and for fast ion orbits of significant width, the resonance condition (2) should be accurately investigated with numerical tools, such as the HAGIS code. Section IV of this paper investigates the structure of the resonances (2) for the experimentally observed tornado modes, which are reproduced with the MISHKA and CASTOR codes.

Section V of this work presents the experimental data obtained from the TOFOR neutron spectrometer. The distribution function of the energetic deuterium ions is reproduced from the nuclear data, and properties of this distribution function are analyzed.

Section VI describes the reconstruction of the unperturbed profile of the fast D ions from the 2D gamma-ray camera.

Section VII of this paper describes results from the HAGIS code on modeling the interaction between fast deuterium ions and tornado and TAE modes. The self-consistent HAGIS model includes all the modes observed before the sawtooth crash interacting with the ICRH-accelerated fast ions. The distribution function of the fast ions is obtained from the fitting to the experimentally measured energy distribution function (neutron spectrum from TOFOR) and to the gamma-ray spatial profile (2D gamma-camera). The resulting re-distribution of the fast ions resonating with TAE/tornado modes is compared then to the experimentally measured data. It is also shown for the first time that the excitation of a tornado mode with negative toroidal mode number could result from fast ion redistribution at the nonlinear phase of TAE instabilities with positive mode numbers. Together with the previous interpretations of the bi-directional tornado modes [28, 27], this effect completes the possible explanations of the experimentally observed modes with negative toroidal mode numbers.

Section VIII summarizes the results presented in this paper.

2. THE EXPERIMENT

The experiments were performed on the JET tokamak [26] (major radius of the magnetic axis $R_0 \approx 2.9$ m, minor radius $a \approx 1$ m, $I = 2$ MA, $B = 2.24$ T, graphite walls, deuterium plasma). Deuterium NBI with energy ~ 110 keV and power waveform of 1.5 MW - 3 MW - 4.5 MW was accelerated by 3 MW of ICRH at the frequency of the 3rd deuterium harmonic, 51 MHz. Both NBI and ICRH were applied after the inductive current fully penetrated and current flat top was established. Discharges were in L-mode during the experiment. Electron density was in the range $2.5 - 3.3 \times 10^{19}$ m^{-3} during the time of interest.

In order to avoid strong absorption of the ICRH power by hydrogen impurity ions in JET plasmas, a careful choice of the magnetic field value, 2.24T was made. At this field, the 3rd D harmonic resonance is close to the magnetic axis and the main region of the beam deposition, while the 1st and 2nd hydrogen harmonic resonances are placed away, as Figure 1 shows. It is clear from this figure that 2nd hydrogen resonance for the magnetic field chosen is driven outside the outer wall of the JET vessel, while the 1st hydrogen resonance is just inside the inner wall and can hardly absorb significant ICRH power in this edge-localized cold plasma.

Figure 2 displays the temporal evolution of the main plasma parameters of interest. One can see that the yield of DD fusion reactions during the NBI only heating (time window $11 - 12$ sec) was increased by a factor of 6 or so when 3 MW of ICRH was applied ($12 - 14$ sec.). Such a significant increase in the rate of DD fusion is explained by the acceleration of D beam ions up to high energy range so the cross-section of the DD reaction increases significantly.

A monster sawtooth is formed in the discharge shown in Figure 2 at $t \approx 14$ sec. A sawtooth-free period in this plasma increases up to ~ 1.54 sec, and the monster sawtooth crash at $t \approx 15.6$ sec causes a drop in central electron temperature from ~ 5 keV to ~ 4 keV. The neutron rate drops at the same time from 9×10^{15} sec^{-1} to 5×10^{15} sec^{-1} and does not recover anymore suggesting a significant decrease in the fast deuteron populations that provides a high cross-section of the DD reaction. Although a number of monster-type sawteeth followed after the main crash at ~ 15.6 sec, it is the time before this crash when time resolved measurements of the fast deuterons are best of all, so we focus our further analysis on the plasma events preceding this main monster crash.

Alfvén activity was monitored in this discharge with Far Infrared (FIR) interferometry and external Mirnov coils mounted just above outer mid-plane and separated in toroidal direction by about 5^0 and 11^0 degrees. This set of the coils is designed to allow detection of magnetic perturbations in the frequency range up to 500 kHz with effective 12 bit amplitude resolution and sensitivity $|\delta B_P/B_0| \approx 10^{-9}$. A number of Alfvén eigenmodes was detected before the monster sawtooth crash. Figures 3 and 4 display the phase magnetic spectrogram and the FIR interferometry spectrogram showing the modes in the TAE frequency range with different toroidal mode numbers excited one-by-one. It is seen that the modes with higher toroidal mode numbers are excited first, with the modes of lower toroidal mode numbers following. This pattern of the TAE excitation is consistent with a gradual decrease of the on-axis safety factor $q(0)$ in time as the current profile peaks after the previous sawtooth crash [10, 3, 29, 28].

Fast ion diagnostics in these JET experiments were represented by:

- Gamma-ray spectrometry [17] measuring the energy spectrum of the gamma-rays from the plasma
- The 19-channel 2D gamma-ray camera measuring total (integrated over energy) emission of gamma-rays [18] along the lines-of-sight, which are shown in Figure 5.
- The fast ion loss detector [2, 20], the scintillator, measuring Larmor radii and pitch-angle of the lost ions just below the outer mid-plane of the machine.
- The neutron time-of-flight spectrometer TOFOR [15] providing data on the energy spectrum of DD neutrons.

The scintillator probe [2, 20], which is located just below the mid-plane of the JET torus outside the plasma, detects lost ions and provides information on the lost ion pitch angle and gyro-radius. The basic principle of scintillator measurements is the emission of light by a scintillator after a fast ion strikes it. An optical system within the scintillator probe is used to transfer the light emitted by the scintillator through a coherent fibre bundle towards a charge-coupled device (CCD) camera and a photomultiplier array.

Gamma-ray emission coming from nuclear reactions between the fast ions and main plasma impurities C and Be constitues a valuable means for observing fast particle redistribution in the plasma core. Spatial profiles of the gamma-ray emission in the energy range $E_\gamma > 1$ MeV were measured using the 2D gamma-ray camera [18], which has 10 horizontal and 9 vertical collimated lines of sight. The detector array is comprised of 19 CsI(Tl) detectors. The data acquisition system accommodates the gamma-ray count-rate measurement in 4 independently adjustable energy windows. This allows gamma-ray peaks for a given fast ion population in specific windows to be counted separately. The special energy window, containing the 3.09 MeV peak with its single and double escape satellites was set up to measure spatial profiles of the gamma-ray emission from D ions. The effective spatial resolution of the diagnostic in these experiments is about ±6 cm. For this particular discharge the relevant nuclear reaction is ^{12}C(d,p)^{13}C, where the energy of the deuteron has to exceed a threshold of ~ 700 keV. The time evolution of the signal in five vertical channels ($14 - 18$) is shown in Figure 6, indicating the redistribution of fast deuterons from the plasma centre to the outside.

Figure 7 presents measurements of the gamma-ray intensity as function of energy during the time preceding the monster sawtooth crash. A peak corresponding to the nuclear reaction ^{12}C(D,p)^{13}C dominates the spectrum of the gamma-rays at 3.09 MeV. A best fit modeling with the GAMMOD code [19] suggests an effective tail temperature of fast deuterons of $\langle T_D \rangle \sim 400$ keV. This estimate is consistent with the threshold energy of about ~ 700 keV required for the fast deuterons to enter the nuclear reaction ^{12}C(D,p)^{13}C. A similar analysis performed for the gamma-ray spectrum after the monster crash, during 14.25 sec - 15.6 sec, shows a somewhat lower averaged energy of the fast deuterons, ~ 320 keV.

A significant difference in the character of the fast ion losses is observed before, during, and after the monster sawtooth crash on the scintillator. Figure 8 shows a much wider region of the phase space, with significantly broader pitch-angle, of the lost ions just before the monster sawtooth crash. The calculated range of the fast deuterons corresponding to the Larmor radii of the fast ion losses observed are in the range from 780 keV to 1.35 MeV. These values confirm the MeV range temperature of the accelerated deuterium beam ions as gamma-ray spectrometry suggests in Figure 7.

By selecting the phase space regions marked in Figure 8 as “Spot 1” and “Spot 2”, one can derive the temporal evolution of the fast ion losses integrated over the 2D areas of these spots. Figure 9 represents the result of such integration. It is seen that fast ion losses in the “Spot 1” phase space region almost double during the tornado mode activity. This increase of the fast ion loss suggests even stronger “loss” of the fast ions from the area inside the $q = 1$ radius, with inevitable decrease of the fast ion stabilization of the sawtooth.

3. MODELING OF MHD-MODES

A suite of MHD codes is employed on JET for modeling the experimentally observed TAE/tornado modes and the internal $n = 1$ kink mode. The aim of the modeling is to reproduce accurately the plasma equilibrium and the temporal evolution of the observed MHD modes with various toroidal mode numbers. Figure 3 shows the experimentally observed TAE and tornado modes detected with the external Mirnov coils. Figure 4 shows tornado modes detected with the FIR interferometry, which has the vertical line-of-sight passing close to the magnetic axis. In contrast to the external Mirnov coils, where the edge-localized TAE obscure significantly the core-localized tornado modes, the interferometry gives a better picture of the tornado modes inside the $q = 1$ radius. In particular, the sequence of the tornado modes appearing one-by-one in time as the on-axis safety factor decreases, can be seen with very good time resolution.

3.1. EQUILIBRIUM RECONSTRUCTION

The equilibrium reconstruction code EFIT combined with the motional Stark effect (MSE) diagnostics for measuring safety factor profile is employed first [4]. This technique of the equilibrium reconstruction on JET provides accuracy of $10\% - 15\%$ for the $q(r)$ - profile. However, to increase the accuracy of determining the value of the on-axis safety factor $q(0)$, and for assessing the temporal evolution $q(r = 0, t)$, the well-known technique [27] based on detecting TAE inside the $q = 1$ radius can be employed. Namely, the observed tornado modes with different toroidal mode numbers n are used by applying the relation between n and the values of $q(r)$ corresponding to magnetic surfaces where TAE reside:

$$q_{TAE} = \frac{m - 1/2}{n} \approx [m \approx nq, q \leq 1] \approx \frac{n - 1/2}{n}. \tag{3}$$

The toroidal mode numbers are identified from the set of toroidally separated Mirnov coils, and the exact timing of the modes appearing one-by-one as $q(r = 0, t)$ decreases, is found from the interferometry diagnostics (see Figures 3 and 4).

Table 1: Times and on-axis values of the safety factor derived from the start of appearance of tornado mode with mode number n.

$\mathbf{n}$	11	10	9	8	7	...	4	3
$\mathbf{q(0)}$	0.955	0.95	0.944	0.938	0.93		0.875	0.833
$\mathbf{t[s]}$	14.35	14.38	14.42	14.5	14.6		14.8	15.05

With the data from tornado modes (compare Table 1), the on-axis value of the safety factor can be extrapolated in time for obtaining the estimate of the on-axis safety factor at the time of the sawtooth crash (15.6 sec):

$$q(r = 0, t = 15.6) \approx 0.791. \tag{4}$$

With the use of this estimate of the on-axis safety factor, the plasma equilibrium is reconstructed by the EFIT+MSE code just before the sawtooth crash and during the interval preceding it, and the straight field line coordinate system is built for this equilibrium with the HELENA code.

3.2. INTERNAL KINK MODE

In the presence of a stabilising energetic particle population inside the $q = 1$ radius, the internal kink instability is described by the quadratic form

$$\gamma^2 I = \delta W_{MHD} + \delta W_K, \tag{5}$$

where $I = \int d^3x\rho|\xi|^2$ is the plasma inertia term, γ is the growth rate of the instability, δW_{MHD} is the ideal MHD contribution to the growth rate due to the thermal plasma, and

$$\delta W_K = -\int d^3x \left[\nabla \cdot \xi_\perp^* \delta p_\perp + (\delta p_\perp - \delta p_\|)(\mathbf{b} \cdot \nabla)\mathbf{b} \cdot \xi_\perp^*\right] \tag{6}$$

is the stabilising contribution due to the fast particle population. Here, ξ is the plasma displacement vector, ρ is the plasma mass density, and $\delta p_\|, \delta p_\perp$ are the fast ion pressure components. When all tornado modes are present from 15.05 s to 15.6 s, both values of δW_{MHD} and δW_K evolve due to the temporal evolution of the $q(r)$-profile, thermal and fast particle pressures. In order to assess the relative change in both MHD and fast particle contributions during the time of interest, we first compute δW_{MHD} in this section, while the effect of fast particles on the kink mode, δW_K, will be discussed in the rest of this paper. The change in δW_{MHD} is estimated by the ideal MHD code MISHKA-1 by directly computing the growth rates of the kink mode at times 15.05 s and 15.6 s. In this approach, assuming that the total plasma pressure is determined by thermal plasma, the ratio of the MHD contributions is

$$\frac{\delta W_{MHD}(t=15.05)}{\delta W_{MHD}(t=15.6)} = \frac{\gamma^2(t=15.05)}{\gamma^2(t=15.6)} \approx 0.76. \tag{7}$$

The accuracy of the spectral MHD code MISHKA-1 could be estimated by using this code for computing AEs and comparing the computed eigenvalues of the AEs to the experimentally observed AE frequencies (see next Section).

3.3. ALFVÉN EIGENMODE MODELING

For estimating δW_K in the presence of Alfvén Eigenmodes (AEs), one first needs to explain the experimentally observed set of AEs. For plasma density nearly constant in time, $n_e(0) = 3 \times 10^{19}\mathrm{m}^{-3}$, and magnetic field $B_T(0) = 2.24\mathrm{T}$, the Alfvén velocity is

$$V_A(0) = 2.18 \times 10^{11} \mu^{-1/2} n_i^{-1/2} B \cdot 10^4 [cm/s] \approx 6.4 \times 10^6 \mathrm{m/s}, \tag{8}$$

and the TAE frequency is

$$\omega_0 = \frac{V_A}{2qR} \approx 1.06 \times 10^6 \mathrm{s}^{-1}; f_0 \equiv \frac{\omega_0}{2\pi} \approx 170\mathrm{kHz}. \tag{9}$$

The toroidal rotation of the plasma driven by uni-directed NBI is measured with the charge-exchange diagnostics showing an on-axis maximum value of

$$\omega_{tor} \approx 4.5 \times 10^4 \mathrm{s}^{-1}; f_{rot}(0) \approx 7.16\mathrm{kHz}. \tag{10}$$

One can see that the experimentally observed frequencies of tornado modes in laboratory reference frame (Figure 3) correspond, within the experimental error bars, to f_0 with the well-known relation

$$f_n^{LAB} = f_0 + n \cdot f_{rot}, \tag{11}$$

where $n \cdot f_{rot}$ is the Doppler shift.

We now use the CSCAS code for computing the radial structure of the Alfvén continuum and compute all TAE/tornado modes observed just before the monster sawtooth crash at $t = 15.6$ s with the MISHKA-1 and CASTOR codes. Figure 10 shows the set of the modes computed, with two different eigenmodes, core-localized, and edge-localized, for toroidal mode numbers $n = 6$ and $n = 8$. In Figure 10, the scalar electrostatic potential of the perturbation, Φ, is shown as a function of radial variable $s = \sqrt{\Psi_{pol}/\Psi_{pol}(edge)} \approx r/a$.

The accuracy of the AE modeling can be estimated now by directly comparing the computed AE eigenfrequencies with the TAE frequencies observed experimentally. Consider, for example, the computed $n = 4$ TAE with eigenfrequency $\omega R_0/V_A(0) = 0.494$ localised at $r/a \approx 0.35$ (see Figure 10). For the plasma parameters mentioned above, the computed mode frequency in the plasma reference frame corresponds to 174 kHz. At the mode localization region, the measured toroidal rotation of the plasma is $\omega_{tor} \approx 3.2 \times 10^4 s^{-1}$, causing a Doppler shift of $nf_{rot} \approx 4\,(3.2 \times 10^4/2\pi) = 20.4$ kHz, so that the computed TAE in the laboratory reference frame in accordance with Eq. (11) would have frequency 194.4 kHz. On the other hand, the experimentally observed $n = 4$ TAE in Figure 3 has a frequency of ~ 190 kHz, deviating less than 3% from the computed one.

4. WAVE-PARTICLE RESONANCES

The fast ion distribution is assumed to be of the form

$$f(E, P_\phi, \Lambda) = f_E(E) f_{P_\phi}(P_\phi) f_\Lambda(\Lambda) \tag{12}$$

with energy E, toroidal angular momentum P_ϕ and the normalized magnetic moment $\Lambda \equiv \mu B_0/E$. Here $\mu = mv_\perp^2/2B$ is the magnetic moment and B_0 is the magnetic field on axis.

Since 3$^{\text{rd}}$ harmonic on-axis ICRH heating was used to accelerate the deuterons, we can investigate resonances of trapped particles that have their turning points vertically above and below the magnetic axis. At the banana tips $v_\parallel = 0$, thus all energy is in the perpendicular motion and $\mu = E/B_0$ there. This can be described by the relation $\Lambda_0 = 1$. The function $f_\Lambda(\Lambda)$ is given by

$$f_\Lambda(\Lambda) = \exp\left(-\frac{(\Lambda - \Lambda_0)^2}{\Delta\Lambda^2}\right), \tag{13}$$

with $\Delta\Lambda = 1.5 \times 10^{-1}$.

Also, for such trapped particles the toroidal angular momentum reduces to $P_\phi \propto -\Psi_{pol}$, where Ψ_{pol} is the poloidal magnetic flux at the position of the turning point, which is a function of Z only. This allows us to look at particle resonances in the reduced space $\{E, \Delta Z\}$, with ΔZ measuring the vertical distance between the orbit at $(R = R_0, Z)$ and the magnetic axis at $(R = R_0, Z = Z_0)$.

Particles with starting positions distributed over the reduced space $\{E, \Delta Z\}$ were followed by HAGIS [23] in the absence of TAEs, and their unperturbed orbit-averaged toroidal precession frequency $\langle\dot{\varphi}\rangle$ and poloidal bounce frequency $\langle\dot{\vartheta}\rangle$ involved in the resonance condition (2)were calculated as functions of energy E and Z.

Recalling the condition for wave-particle resonance (2) one can introduce the quantity $log(1/\Omega)$ as a measure for the resonance, the higher the value, the closer a point in phase space is to the mode-particle resonance.

In order to see whether the interaction of the fast deuteron population with Alfvénic modes may lead to a significant redistribution, which will result in a changed gamma ray emission profile, we combine the information of the reaction cross section, the fast particle distribution in energy as well as in radius and the position of resonances.

Combining the resonance plots with both cross section and distribution function leads to some insight concerning possible particle redistribution due to wave-particle interaction. Figure 11 shows a contour plot of $f\langle v\sigma\rangle \log(1/\Omega)$ as function of energy and vertical distance. Around 900 keV as well as around 1100 keV several resonance lines cross an area of high reaction rate for the fast D ions and carbon impurity giving the gamma-rays of interest. If a transport of fast deuterons occurs across this resonance lines outwards in radial direction a significant reduction in gamma ray production rate is to be expected due to the particle redistribution away from the (hot) plasma centre.

5. NEUTRON SPECTRUM AND DERIVED FAST ION DISTRIBUTION

Using data measured by the TOFOR [15] neutron time-of-flight spectrometer it is possible to reconstruct the energy dependence of the fast deuteron distribution for this experiment. For performing such a reconstruction, two important conditions are used: the special vertical line-of-sight of TOFOR, and the strong temperature anisotropy, $T_\perp \gg T_\parallel$, of the fast D distribution function accelerated with ICRH. The time of flight t_{TOF} for a neutron is proportional to $1/\sqrt{E_n}$, where E_n is the neutron energy.

The measured time-of-flight data, together with the spectral components that are fitted to the data in order to reconstruct the energy distribution function, is depicted in Figure 12.

Measuring the time of flight spectrum thus allows calculating the energy spectrum, from which the energy distribution of fast deuterons has been deduced. Also, an analytical solution of the Fokker-Planck equation describing the acceleration of the beam deuterons by the 3rd harmonic ICRH heating scheme was calculated, which nicely fits the reconstructed profile [11, 12]. For our simulations we thus employ the analytical solution as $f_E(E)$ which is shown in Figure 13.

6. UNPERTURBED PROFILE OF FAST D IONS RECONSTRUCTED FROM 2D GAMMA-RAY CAMERA

In order to find the function f_{P_ϕ} we proceed as follows: The data from horizontal and vertical gamma channels at a time just before the onset of the TAE and tornado modes (timeslice 13.83 s) is the reference we compare our starting distribution against. For a range of different f_{P_ϕ}-profiles we simulate the gamma emission and compare it to the experimental data. The profile that provides the best fit is chosen as our fast deuteron distribution function. This best fit is shown in Figure 14.

The absolute scaling of the distribution function is determined by matching the fast ion energy content W_{fast} of our model distribution with the value obtained in calculations , $W_{fast} = 0.57$ MJ.

It should be noted that HAGIS is a guiding centre code, i.e. it doesn't take into account finite Larmor radius (FLR) effects. The mean energy for D ions contributing to the gamma signal is ~ 1.5 MeV. At this energy the Larmor radius is ~ 24 cm, which spans up to three camera channels. Some simulations were made to investigate how the gyro-motion affects the camera signal. The camera response for several trial distributions has been tested with and without considering FLR effects, and the overall results are very similar for the two cases. The only exception is channel 15, which generally gets fewer counts ($\sim 15 - 20\%$) due to the finite Larmor radius.

7. MODELING RESULTS

The distribution function given by Equation (12), (with parameters as determined in Section IV) was used in self consistent simulations with the HAGIS code. A total number of nine modes, whose Eigenfunctions have been calculated in the CASTOR code, have been used in this modeling effort. The range of toroidal mode numbers is $n = 3-8$ as well as $n = -4$. For the mode numbers $n = 6$ and $n = 8$ a localized tornado mode inside the $q = 1$ surface as well as a global TAE mode were found and employed in the simulation.

In the experiment, the modes appear one-by-one following a gradual decrease of $q(0)$ caused by the diffusion of the plasma current on a resistive time scale. Since the HAGIS code is optimized for computing accurately wave-particle interaction on Alfvén time scale, which is much shorter than the transport time scale, the time constraint of the numerical modeling does not allow computing the whole long temporal evolution of the fast D ions in the presence of modes appearing one-by-one. Instead, the HAGIS code is employed for investigating in detail the crucial moment just before the monster sawtooth crash, when all TAE and tornado modes are observed together (at time slice 15.6 s).

The simulation was run long enough to ensure saturation for the strongest modes, allowing for complete redistribution of the fast ion population. The time evolution of the mode amplitudes in this simulation is presented in Figure 15.

It is evident that the counter-propagating mode with $n = -4$ is well excited. However, a simulations with this $n = -4$ mode alone (i.e. in the absence of all other modes) has shown this mode to be stable. This suggests that a nonlinear coupling of the counter-propagating mode with co-propagating $n > 0$ modes via a fast particle distribution may cause the drive needed for the $n < 0$ mode.

Apart from the evolution of the mode amplitudes HAGIS also provides information on the redistribution of a fast ion population due to the influence of MHD-modes. In Figure 16 the change in particle density is shown as a function of the radial coordinate $s = \Psi_{pol}/\Psi_{pol,edge}$ and time. Here Ψ_{pol} denotes the poloidal flux and $\Psi_{pol,edge}$ is the value of the poloidal flux at the plasma edge. The redistribution from the plasma centre towards outer regions is apparent.

A nuclear reaction module in HAGIS allows studying the redistribution occurring in simulations by means of synthetic diagnostics. Providing density and temperature profiles for plasma impurities that form a reactant in the nuclear reaction ^{12}C(D,p)^{13}C, as well as the cross section for this reaction, it is possible to calculate the reaction rate.

This data is then employed for evaluating the integrals along the lines-of-sight of the JET gamma-camera, enabling a direct comparison with the 2D experimental data. The redistributions of the fast D ions modeled and observed via gamma-ray intensity with the JET gamma-camera are depicted in Figure 17, showing how well the measured and simulated redistributions agree.

Further we investigated the stability of the $n = 1$ internal kink mode that constitutes the sawtooth instability. Recalling the expression (5), we have to investigate the changes in the ideal MHD contribution δW_{MHD} and the fast particle contribution δW_K during the time 15.05 s and 15.6 s, when all TAE/tornado modes are present.

For the relative change in the MHD contribution we find (compare Section III.B)

$$\frac{\delta W_{MHD}(t = 15.6s) - \delta W_{MHD}(t = 15.05s)}{\delta W_{MHD}(t = 15.05s)} \approx 0.32. \tag{14}$$

The relative change in the stabilising fast particle contribution δW_K in the time of interest is calculated in HAGIS as

$$\frac{|\delta W_K(t = 15.6s)| - |\delta W_K(t = 15.05s)|}{\delta W_{MHD}(t = 15.05s)} \approx -0.25. \tag{15}$$

So while the ideal MHD contribution δW_{MHD} to the growth rate increases by about 30%, the magnitude of the stabilising part δW_K decreases, and is thus less capable of countering the destabilization. Destabilization is obtained when the redistribution caused by the interaction with the Alfvénic modes is taken into account.

8. SUMMARY

JET discharge # 74951, in which neutral beam injected deuterons were accellerated to energies in the MeV range by 3rd harmonic ICRF heating has been investigated. This experiment allows for an exhaustive analysis of fast particle redistribution due to MHD modes because of the advanced diagnostics used. These include the gamma-ray spectrometer, 2D gamma-camera, scintillator probe and time-of-flight neutron spectrometer TOFOR.

The experimental data focuses on the population of high energy deuterons, produced by accelerating neutral beam injected particles by 3rd on-axis ICRH. On the one hand these highly energetic particles provide stabilizition for the $n = 1$ internal kink mode that constitutes the observed sawtooth instability, on the other hand they serve as a source of free energy for driving a range of TAE and tornado mode. It is the particular combination of NBI and ICRH that creates a fast ion population with such characteristic traits. When the value of the safety factor at the magnetic axis, $q(0)$, drops below 1, the Alfvénic modes begin to appear one by one, driven by the fast deuterons. This leads to an outward redistribution of the fast ion population from inside the $q = 1$ surface. Upon reducing the number of high energy deuterons inside the $q = 1$ radius, the sawtooth stabilization is lost, and subsequently a monster sawtooth crash happens.

With a suite of codes the equilibrium and the linear Eigenfunctions of the modes involved have been reconstructed, forming the initial point for self consistent modlling with the HAGIS code. The initial fast ion distribution function for this simulation was derived from measured data.

Our modeling adequately reproduces the major features of this experiment. It shows that the fast ion population can drive the Alfvénic modes unstable, consequently leading to redistribution of the extent necessary to explain the observed changes in the gamma-ray intensity profiles as well as the loss of fast particle stabilization for the $n = 1$ kink mode.

ACKNOWLEDGMENTS

This work was supported by EURATOM and carried out within the framework of the European Fusion Development Agreement. The views and opinions expressed herein do not necessarily reflect those of the European Commission.

REFERENCES

[1] A. B. Mikhailovskii. Thermonuclear ”drift” instabilities. *Sov. Phys. JETP*, 41:890, 1975.

[2] S. Baeumel, A. Werner, R. Semler, S. Mukherjee, D. S. Darrow, R. Ellis, F. E. Cecil, L. Pedrick, H. Altmann, V. Kiptily, , and J. Gafert. Scintillator probe for lost alpha measurements in jet. *Rev. Sci. Instrum.*, 75:3563, 2004.

[3] S. Bernabei, M. G. Bell, R. V. Budny, E. D. Fredrickson, N. N. Gorelenkov, J. C. Hosea, R. Majeski, E. Mazzucato, C. K. Phillips, G. Schilling, and J. R. Wilson. Nature of monster sawteeth and their relationship to alfvén instabilities in tokamaks. *Phys. Rev. Lett.*, 84(6):1212, 2000.

[4] M. Brix, N. C. Hawkes, A. Boboc, V. Drozdov, S. E. Sharapov, and JET-EFDA Contributors. Accuracy of efit equilibrium reconstruction with internal diagnostic information at jet. *Rev. Sci. Instruments*, 79:10F325, 2008.

[5] C. Z. Cheng and Liu Chen and M. S. Chance. High-n ideal and resistive shear Alfvén waves in tokamaks. *Ann. Phys.*, 161:21, 1985.

[6] D. J. Campbell, D. F. H. Start, J. A. Wesson, D. V. Bartlett, V. P. Bhatnagar, M. Bures, J. G. Cordey, G. A. Cottrell, P. A. Dupperex, A. W. Edwards, C. D. Challis, C. Gormezano, C. W. Gowers, R. S. Granetz, J. H. Hammen, T. Hellsten, J. Jacquinot, E. Lazzaro, P. J. Lomas, N. Lopes Cardozo, P. Mantica, J. A. Snipes, D. Stork, P. E. Stott, P. R. Thomas, E. Thompson, K. Thomsen, and G. Tonetti. Stabilization of sawteeth with additional heating in the jet tokamak. *Phys. Rev. Lett.*, 60(21):2148, 1988.

[7] L. Chen. Theory of magnetohydrodynamic instabilities excited by energetic particles in tokamaks. *Phys. Plasmas*, 1:1519, 1994.

[8] G. Y. Fu and J. W. Van Dam. Excitation of the toroidicity-induced shear Alfven eigenmode by fusion alpha particles in an ignited tokamak. *Phys. Fluids B*, 1(10):1949, 1989.

[9] T. Fulop, M. Lisak, Ya. I. Kolesnichenko, and D. Anderson. Finite orbit width stabilizing effect on toroidal Alfven eigenmodes excited by passing and trapped energetic ions. *Plasma Phys. Control. Fusion*, 38:811, 1996.

[10] W. W. Heidbrink, E. D. Fredrickson, T. K. Mau, C. C. Petty, R. I Pinsker, M. Porkolab, and B. W. Rice. High harmonic ion cyclotron heating in DIII-D: Beam ion absorption and sawtooth stabilization. *Nucl. Fusion*, 39:1369, 1999.

[11] C. Hellesen, M. Gatu Johnson, E. Anderson Sundén, S. Conroy, G. Ericsson, E. Ronchi, H. Sjöstrand, M. Weiszflog, G. Gorini, M. Tardocchi, T. Johnson, V.G. Kiptily, S.D. Pinches, S.E. Sharapov, and JET-EFDA Contributors. Neutron emission generated by fast deuterons accelerated with ion cyclotron heating at JET. *Nucl. Fusion*, 50:022001, 2010.

[12] C. Hellesen, M. Gatu Johnson, E. Andersson Sundén, S. Conroy, G. Ericsson, J. Eriksson, G. Gorini, T. Johnson, V. G. Kiptily, S. D. Pinches, S. E. Sharapov, H. Sjöstrand, M. Nocente, M. Tardocchi, M. Weiszflog, and JET-EFDA Contributors. Measurements of fast ions and their interactions with MHD activity using neutron emission spectroscopy. *Nucl. Fusion*, 50:084006, 2010.

[13] G. T. A. Huysmans, J. P. Goedbloed, and W. Kerner. . In *Proc. CP90 Conf. Comp. Phys.*, 1991.

[14] ITER Physics Basis Editors, ITER Physics Expert Group Chairs and Co-Chairs, and ITER Joint Central Team and Physics Integration Unit. ITER Physics Basis. *Nucl. Fusion*, 39:2137, 1999.

[15] M. Gatu Johnson, L. Giacomelli, A. Hjalmarsson, J. Kállne, M. Weiszflog, E. Andersson Sundén, S. Conroy, G. Ericsson, C. Hellesen, E. Ronchi, H. Sjóstrand, G. Gorini, M. Tardocchi, A. Combo, N. Cruz, J. Sousa, S. Popovichev, and JET-EFDA Contributors. The 2.5-MeV neutron time-of-flight spectrometer TOFOR for expreiments at JET. *Nucl. Instrum. Methods A*, 591:417, 2008.

[16] W. Kerner, J. P. Goedbloed, G. T. A. Huysmans, S. Poedts, and E. Schwarz. CASTOR: Normal-Mode Analysis of Resistive MHD Plasmas. *J. Comput. Phys.*, 142:271, 1998.

[17] V. G. Kiptily, F. E. Cecil, and S. S. Medley. Gamma ray diagnostics of high temperature magnetically confined fusion plasmas . *Plasma Phys. Control. Fusion*, 48:R59, 2006.

[18] V.G. Kiptily, J.M. Adams, L. Bertalot, A. Murari, S.E. Sharapov, V. Yavorskij, B. Alper, R. Barnsley, P. de Vries, C. Gowers, L.-G. Eriksson, P.J. Lomas, M.J. Mantsinen, A. Meigs, J.-M. Noterdaeme, F.P. Orsitto, and JET-EFDA Contributors. Gamma-ray imaging of D and 4He ions accelerated by ion-cyclotron-resonance heating in JET plasmas. *Nucl. Fusion*, 45:L21, 2005.

[19] V.G. Kiptily, F.E. Cecil, O.N. Jarvis, M.J. Mantsinen, S.E. Sharapov, L. Bertalot, S. Conroy, L.C. Ingesson, T. Johnson, K.D. Lawson, S. Popovichev, and Contributors to the EFDA-JET Workprogramme. γ-ray diagnostics of energetic ions in JET. *Nucl. Fusion*, 42:999, 2002.

[20] V.G. Kiptily, C.P. Perez von Thun, S.D. Pinches, S.E. Sharapov, D. Borba, F.E. Cecil, D. Darrow, V. Goloborod'ko, T. Craciunescu, T. Johnson, F. Nabais, M. Reich, A. Salmi, V. Yavorskij, M. Cecconello, G. Gorini, P. Lomas, A. Murari, V. Parail, S. Popovichev, G. Saibene, R. Sartori, D.B. Syme, M. Tardocchi, P. de Vries, V.L. Zoita, and JET-EFDA Contributors. Recent progress in fast ion studies on jet. *Nucl. Fusion*, 49:065030, 2009.

[21] G. J. Kramer, S. E. Sharapov, R. Nazikian, N. N. Gorelenkov, and R. V. Budny. Observation of odd toroidal alfvén eigenmodes. *Phys. Rev. Lett.*, 92(1):015001, 2004.

[22] A. B. Mikhailovskii, G. T. A. Huysmans, W. O. K. Kerner, and S. E. Sharapov. Optimization of Computational MHD Normal-Mode Analysis for Tokamaks. *Plasma Phys. Reports*, 23:844, 1997.

[23] S. D. Pinches, L. C. Appel, J. Candy, S. E. Sharapov, H. L. Berk, D. Borba, B. N. Breizman, T. C. Hender, K. I. Hopcraft, G. T. A. Huysmans, and W. Kerner. The HAGIS self-consistent nonlinear wave-particle interaction model. *Comp. Physics Comm.*, 111:133, 1998.

[24] F. Porcelli. Fast particle stabilisation. *Plasma Phys. Control. Fusion*, 33(13):1601, 1991.

[25] F. Porcelli, D. Boucher, and M. N. Rosenbluth. Model for the sawtooth period and amplitude. *Plasma Phys. Control. Fusion*, 38:2163, 1996.

[26] P. H. Rebut and B. E. Keen. . *Fusion Technol.*, 11:13, 1987.

[27] M. Saigusa, H. Kimura, Y. Kusama, G. J. Kramer, T. Ozeki, S. Moriyama, T. Oikawa, Y. Neyatani, and T Kondoh. Systematic study of toroidicity-induced Alfven eigenmodes at low-q discharges in JT-60U. *Plasma Phys. Control. Fusion*, 40:1647, 1998.

[28] P. Sandquist, S. E. Sharapov, M. Lisak, T. Johnson, and JET-EFDA Contributors. Bidirectional tornado modes on the Joint European Torus. *Phys. Plasmas*, 14:122506, 2007.

[29] S. E. Sharapov, B. Alper, F. Anderson, Yu. F. Baranov, H. L. Berk, L. Bertalot, D. Borba, C. Boswell, B. N. Breizman, R. Buttery, C. D. Challis, M de Baar, P. de Vries, L.-G. Eriksson, A. Fasoli, R. Galvao, V. Goloborod'ko, M. P. Gryaznevich, R. J. Hastie, N. C. Hawkes, P. Helander, V. G. Kiptily, G. J. Kramer, P. J. Lomas, J. Mailloux, M. J. Mantsinen, R. Martin, F. Nabais, M. F. Nave, R. Nazikian, J.-M. Noterdaeme, M. S. Pekker, S. D. Pinches, T. Pinfold, S. V. Popovichev, P. Sandquist, D. Stork, D. Testa, A. Tuccillo, I. Voitsekhovich, V. Yavorskij, N. P. Young, F. Zonca, JET-EFDA Contributors, and the MAST Team. Experimental studies of instabilities and comfinement of energetic particles on JET and MAST. *Nucl. Fusion*, 45:1168, 2005.

[30] D. J. Sigmar, C. T. Hsu, R. White, and C. Z. Cheng. Alpha-particle losses from toroidicity-induced Alfvén eigenmodes. Part II: Monte Carlo simulations and anomalous alpha-loss processes. *Phys. Fluids B*, 4:1506, 1992.

[31] R. B. White and M. S. Chance. Hamiltonian guiding center drift orbit calculation for plasmas of arbitrary cross section. *Phys. Fluids*, 27:2455, 1984.

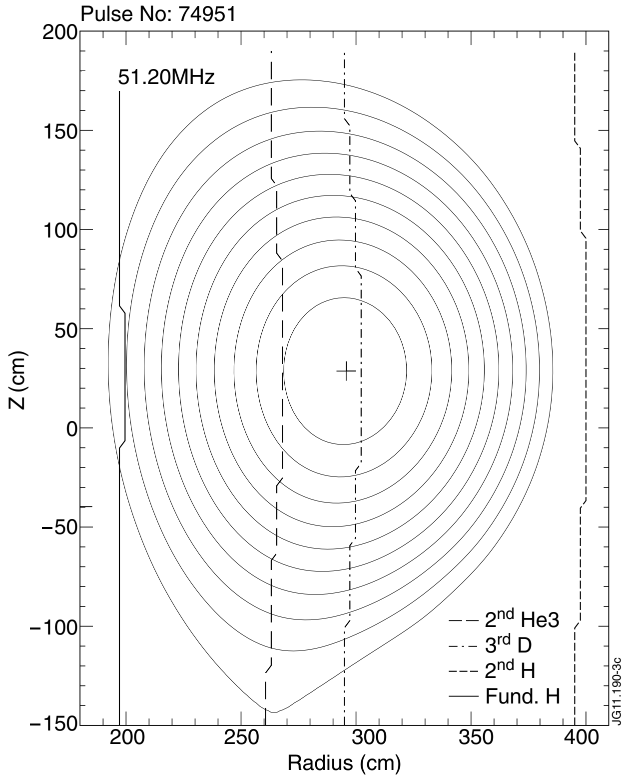

Figure 1: Cross section of JET plasma (B = 2.24T, I = 2MA) showing magnetic flux surfaces and the positions of the main harmonics of cyclotron resonances.

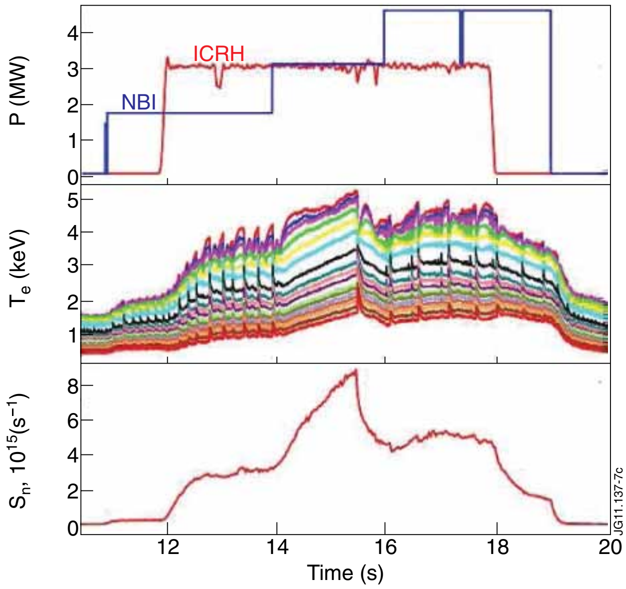

Figure 2: (Color online) Top: Power waveforms of ICRH and NBI in JET Pulse No: 74951. Middle: Temporal evolution of electron temperature measured with multi-channel ECE. Central channel corresponds to ECE measurement of electron temperature at R = 3.03m, edge channel corresponds to R = 3.68m, and the sawtooth inversion radius is at R = 3.35m. Bottom: temporal evolution of the rate of DD neutrons.

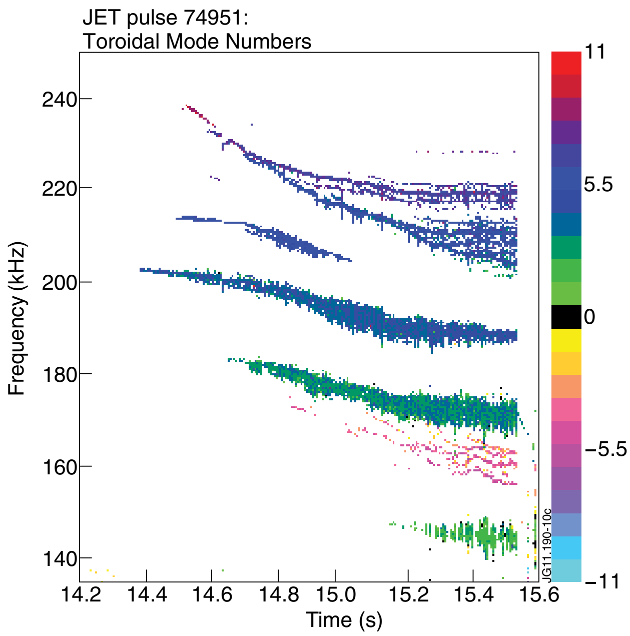

Figure 3: (Color online) Toroidal mode numbers of TAE/tornado modes detected with external Mirnov coils in JET Pulse No: 74951 just before the monster sawtooth crash. Modes with different toroidal mode numbers are identified as: n = 3 − 8 and n = −4.

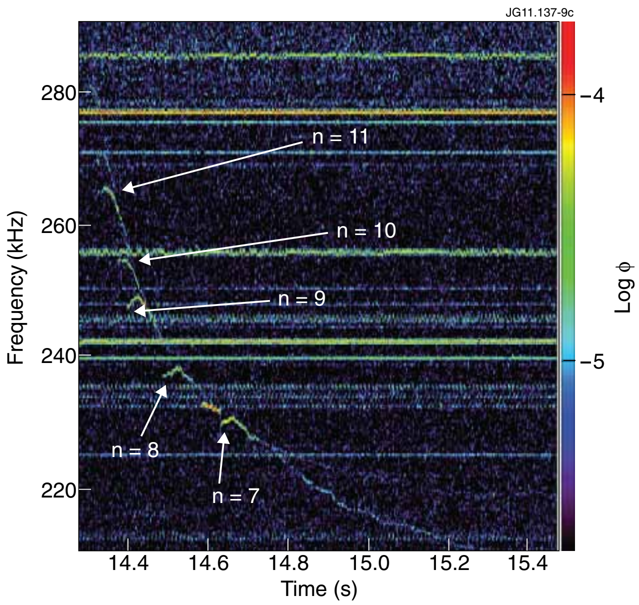

Figure 4: (Color online) Tornado modes with toroidal mode numbers decreasing one-by-one detected with FIR interferometry (line-of-sight through the magnetic axis) in JET Pulse No: 74951.

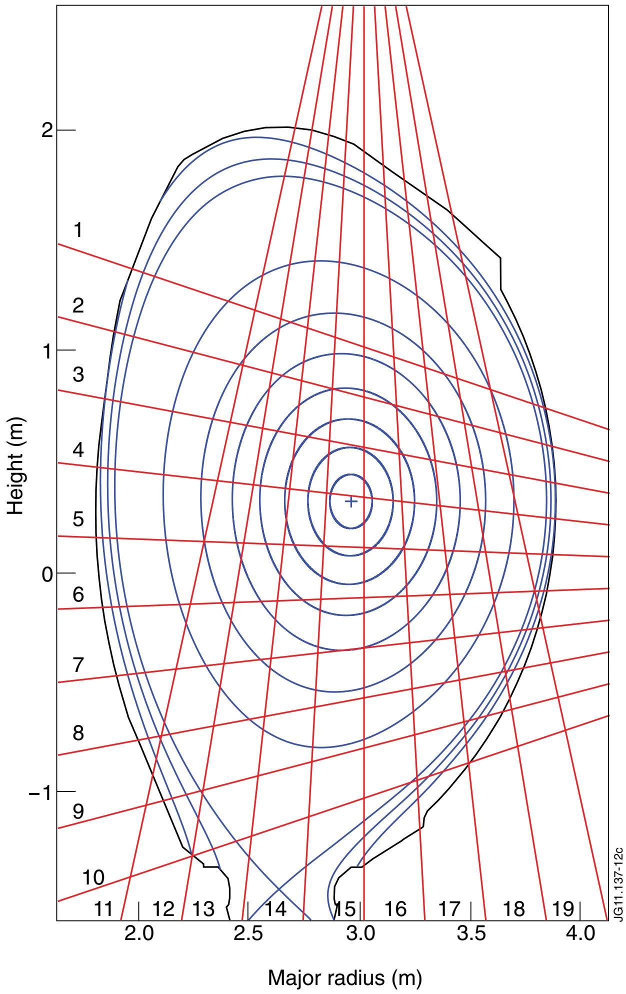

Figure 5: (Color online) Lines-of-sight of the 2D gamma-camera system in JET.

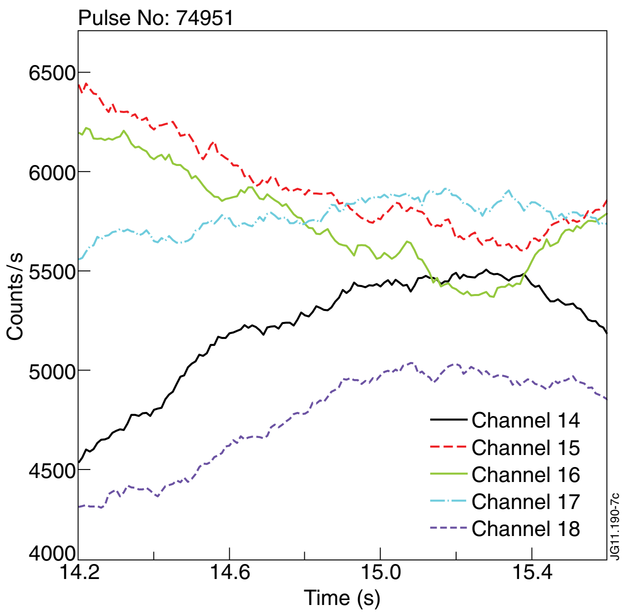

Figure 6: (Color online) Time evolution of the gamma-ray signals for channels 14 - 18 in JET Pulse No: 74951 in the time of interest. The signals in central channels (15, 16) are decreasing, while the signals in outer channels (14, 18) increase, showing the redistribution of gamma-rays from energetic deuterons during observed Alfvénic modes.

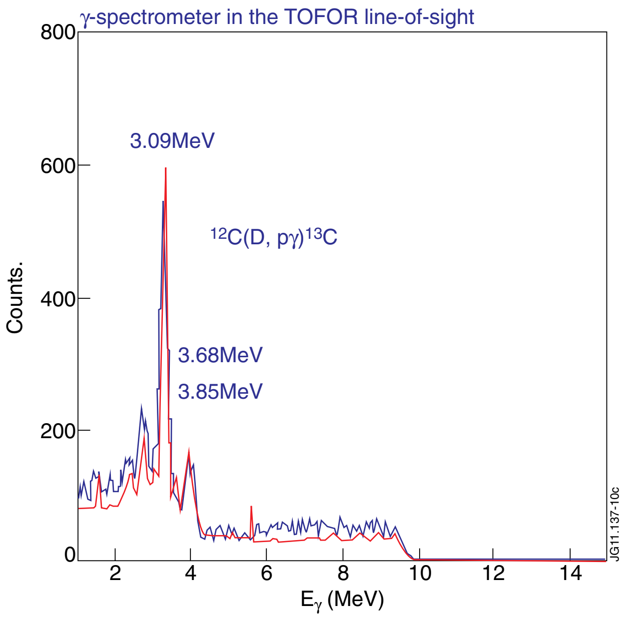

Figure 7: (Color online) Blue: gamma-ray spectrum, dN/dE, as function of gamma-ray energy (in MeV) measured with the gamma-ray spectrometer [19] in JET Pulse No: 74951 and integrated over time interval 12.5 - 14.25 sec. Red: best fit made with the GAMMOD code and an effective tail temperature of fast deuterons $\langle T_D \rangle \approx 400$keV.

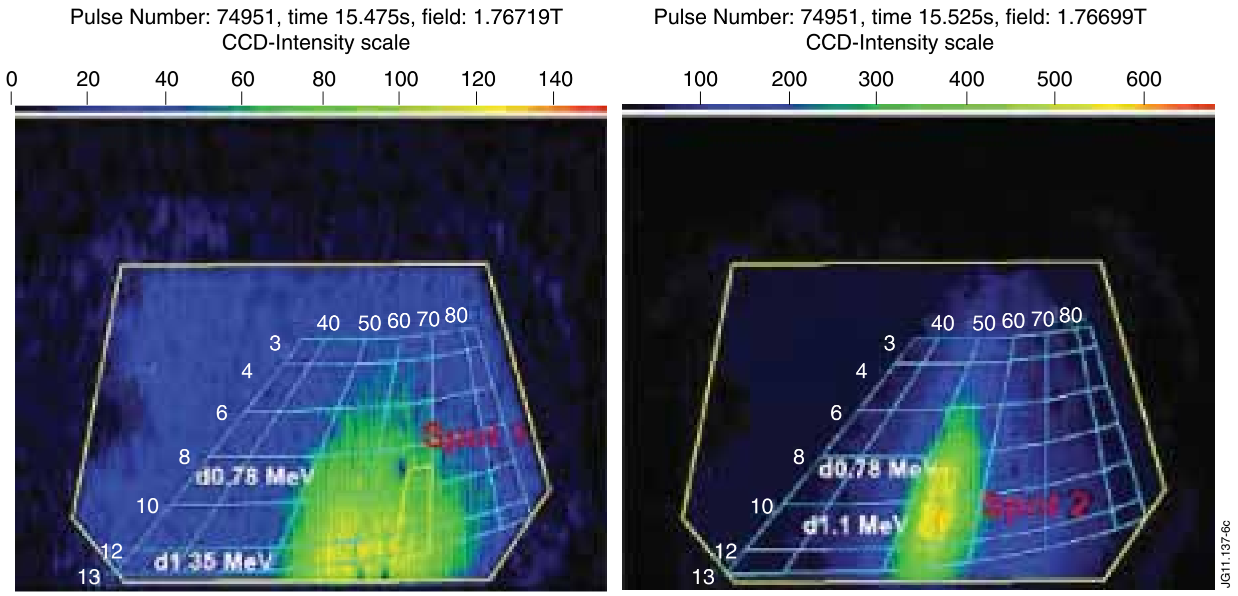

Figure 8: (Color online) Color-coded intensity of the fast ion losses measured with the scintillator probe on the 2D plane of the pitch-angle (in degrees) and Larmor radius (in cm).

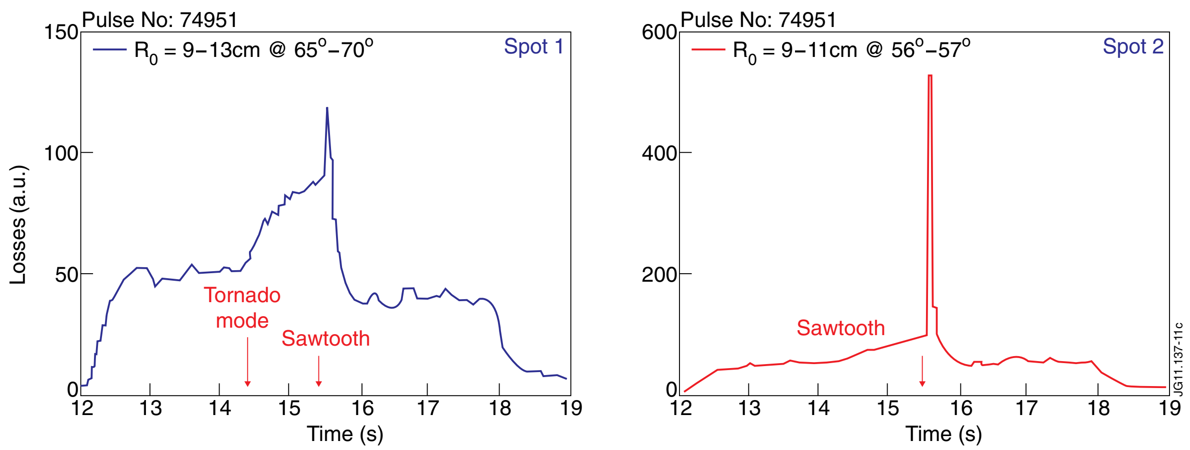

Figure 9: (Color online) Temporal evolution of fast ion losses in the phase regions corresponding the 2D areas of "Spot 1" and "Spot 2" in Figure 8.

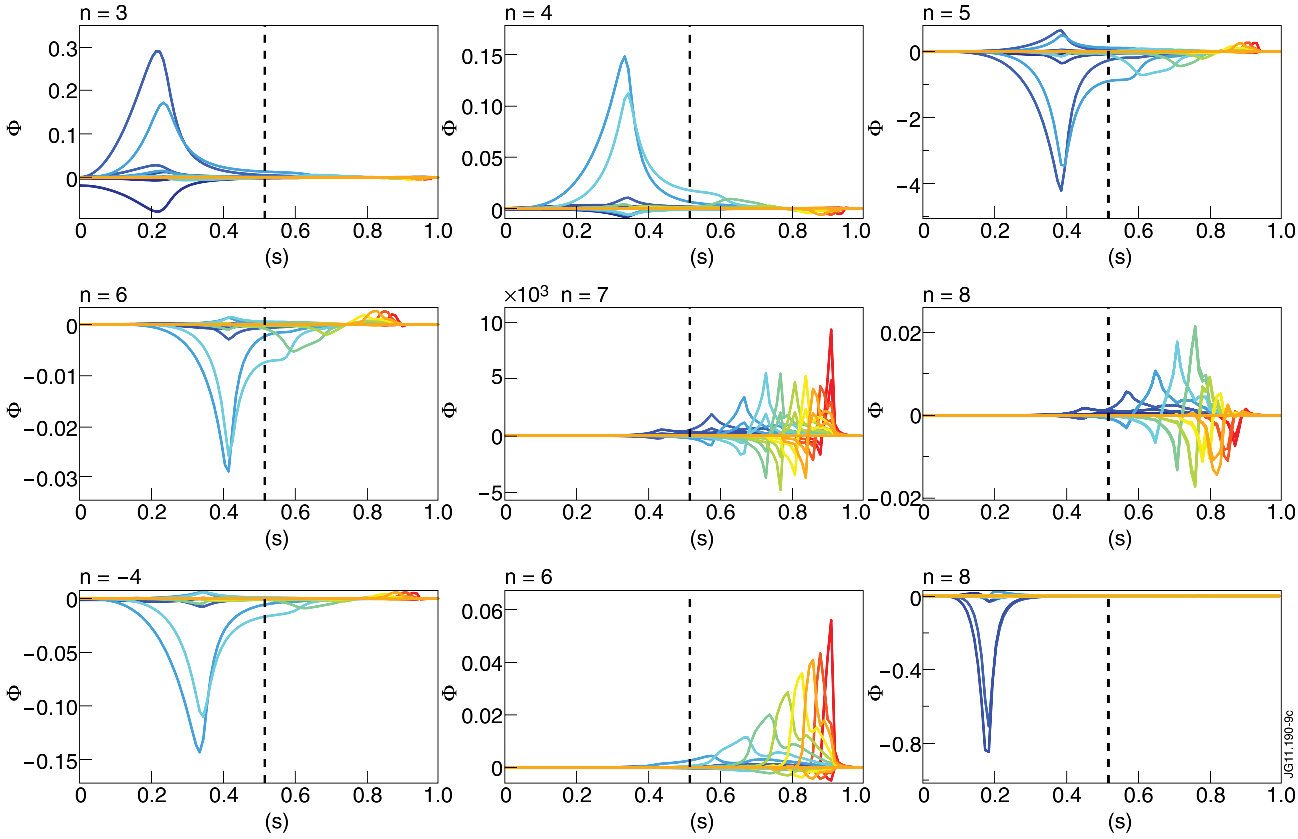

Figure 10: (Color online) The set of TAE/tornado modes computed with the CASTOR code for modeling JET Pulse No: 74951. The dashed black line indicates the position of the q = 1 surface.

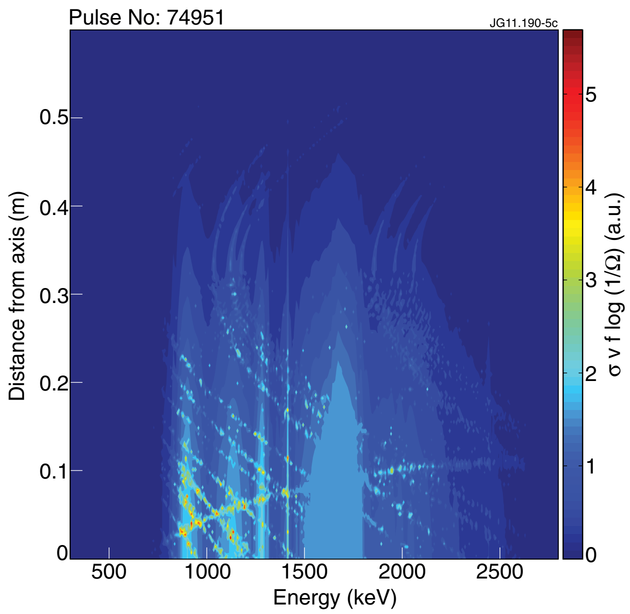

Figure 11: (Color online) The plot of $f(E, s)\langle\sqrt{E}\sigma\ (E)\rangle\ \log(1/\Omega)$ as function of energy and vertical distance from the plasma centre indicates potential areas of large particle redistribution and corresponding gamma rate reduction.

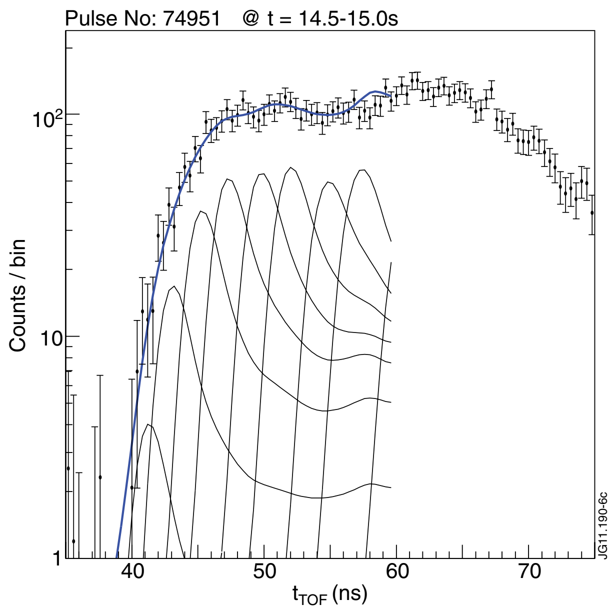

Figure 12: Time-of-flight data for neutrons measured with the TOFOR spectrometer in JET Pulse No: 74951. In addition, the spectral components that are fitted to the data for reconstructing the fast deuteron distribution are shown (thin lines), their sum is shown as a thick line. Every point in the resulting energy distribution (Figure 13) is represented by one spectral component.

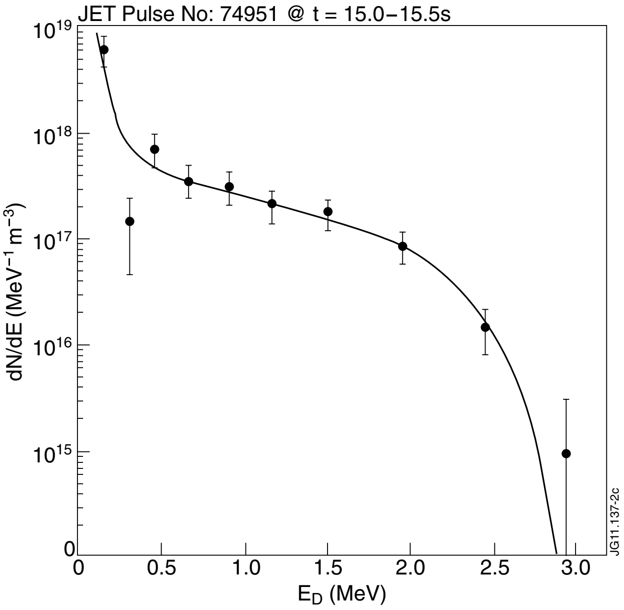

Figure 13: Dependence of the fast deuteron distribution on energy as derived from neutron time-of-flight data measured by TOFOR. The solid line shows the analytical solution of the one-dimensional Fokker-Planck equation.

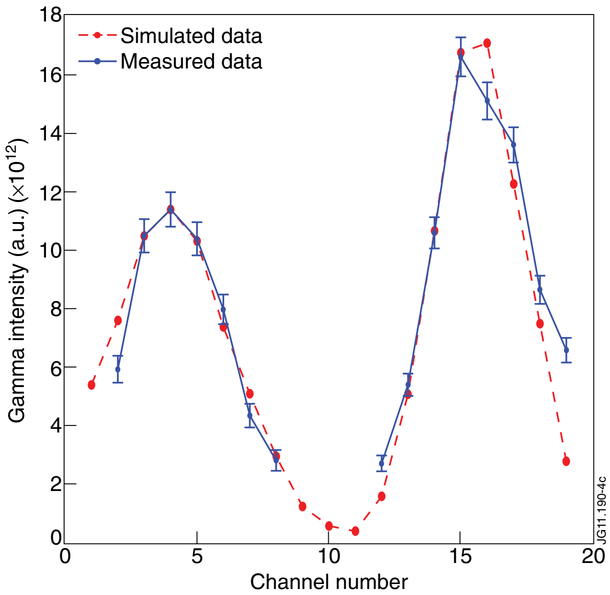

Figure 14: (Color online) Comparison of line-integrated gamma-ray intensities measured with gamma-cameras (horizontal channels: 2-8, vertical channels: 12-19) at time 13.83sec (solid line) with the simulated data for the best fitting profile f_{P_ϕ} (dashed line).

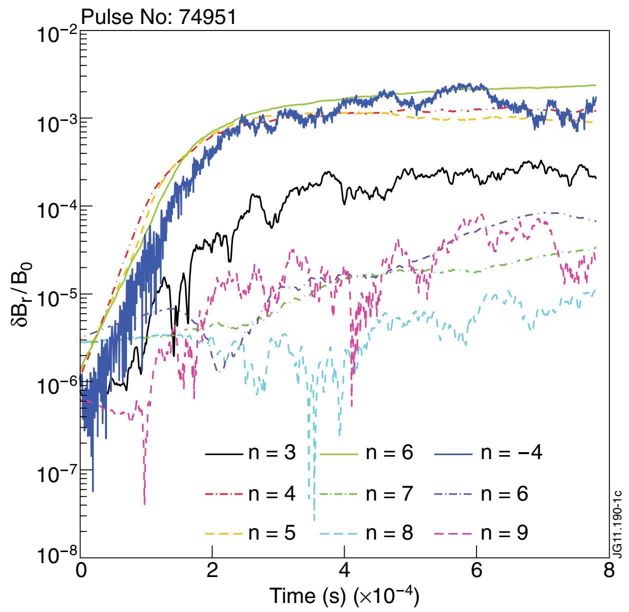

Figure 15: (Color online) Logarithmic plot of the amplitudes $\delta r/B_0$ of the ensemble of TAE and tornado modes in JET Pulse No: 74951 against time obtained from a self-consitent simulation in HAGIS.

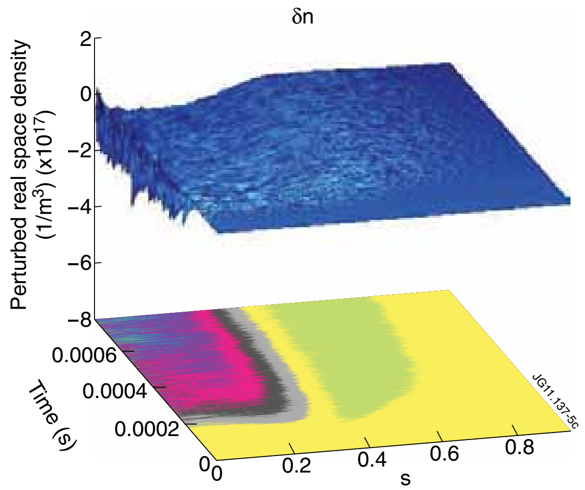

Figure 16: (Color online) The perturbed real space particle density as a function of the radial coordinate s and time in a selfconsistent HAGIS simulation of JET Pulse No: 74951. Particles are removed from the centre and relocated towards the outer regions of the plasma.

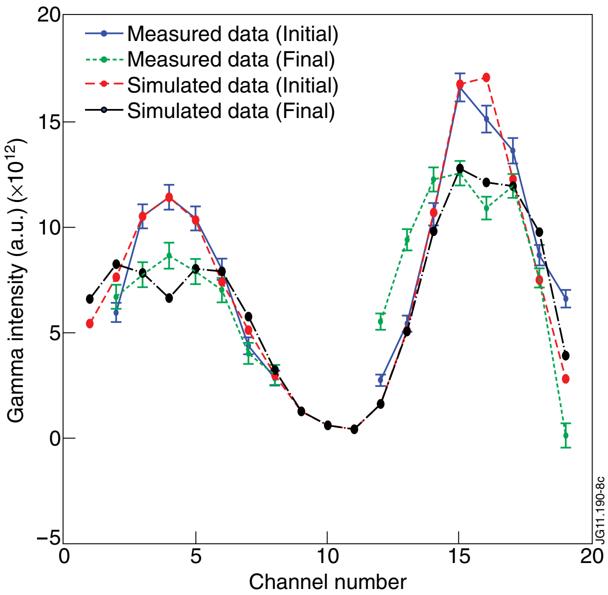

Figure 17: (Color online) Gamma intensity in the 19 channels on JET in Pulse No: 74951. Here we show measured data before (blue) and after (green) redistribution due to interaction with the ensemble of TAE and tornado modes. Simulated gamma intensity is shown in red (initial data) and black (after redistribution).